Antenna Position Layout and Frequency Impact on Tumor Detection in Microwave Breast Imaging

Raquel A. Martins¹, João M. Felício^{1,2}, Jorge R. Costa^{1,3}, Carlos A. Fernandes¹

¹ Instituto de Telecomunicações, IST, Universidade de Lisboa, Lisboa, Portugal, raquel.martins@lx.it.pt

² Centro de Investigação Naval (CINAV), Escola Naval, Instituto Universitário Militar, Almada, Portugal

³ ISCTE – Instituto Universitário de Lisboa (ISCTE-IUL), Lisboa, Portugal

Abstract—We present a systematic study in which we assess the antenna position layout and frequency point distribution of a MWI system, that can potentially improve tumor detection and minimize acquisition time. To this end, we performed measurements on a dry MW setup, using a slot-based antenna in the [2-5] GHz frequency range to scan an anthropomorphic breast phantom, with two different tumor positions, for 40 angular positions. Imaging and tumor-to-clutter ratio metric showed that there is a specific number of angular positions and frequency points beyond which the quality of imaging results does not increase substantially. We found the optimal frequency band for this kind of setup and that the use of lower frequencies seems more beneficial than the use of higher ones. Moreover, distributions of antenna position other from the regular circular one, should be explored further since it showed a decrease of imaging artefacts.

Index Terms—breast cancer diagnosis, microwave imaging, radar imaging, dry microwave setup, ultrawideband antennas.

I. Introduction

For the past years, Microwave Imaging (MWI) has been explored as a complement to conventional imaging techniques for breast cancer screening, such as mammography, ultrasound, and magnetic resonance (MRI). This is due to its ability of being non-invasive, non-ionizing and low-cost [1]-[4].

Microwave (MW) systems may be used in a radar-type configuration [4] where one or several antennas illuminate the breast and receive the echoes back originated from the contrast between the dielectric properties of benign and malignant tumors.

In the case where only one antenna i is rotating around the breast, those systems are called monostatic and retrieve the backscattering response s_{ii} . Most monostatic systems in the literature work in the same manner. However, there are two main aspects where they usually vary: the antennas and the frequency band. In terms of antennas, the variability comes from the antenna itself, the number of angular positions or its distribution around the breast. In respect to the frequency band, the number of frequency points and the width of the frequency band are the two variants.

The duration of a medical exam (scan) in the topic of microwave breast screening is of extreme importance and both aspects can have a high impact on its duration. To our knowledge, there is no organized study on these two aspects, to understand what are the possible optimal configurations that can potentially improve MWI quality, and consequently tumor detection, keeping the acquisition time as short as possible.

Therefore, the goal of this paper is to provide a systematic study to understand more in detail if we can adapt specific antenna and frequency configurations to our advantage. In particular, we focus on the number of angular positions and its layout, and on the number of frequency points and bandwidth.

II. EXPERIMENTAL SETUP

This section briefly describes the MWI experimental setup, including the antenna, fabrication of breast and tumor phantoms, and the image reconstruction algorithm and metrics applied in this work.

A. Microwave imaging setup

As depicted in Fig. 1, this work is based on an experimental dry MW setup [4] that applies a monostatic single-antenna configuration, which scans around a breast phantom, in the z-plane. We used a crossed-exponentially tapered slot-based antenna (XETS) [5] displayed in Fig. 1 (b), working in the [2-5] GHz frequency range (151 points) and connected to a vector network analyzer.

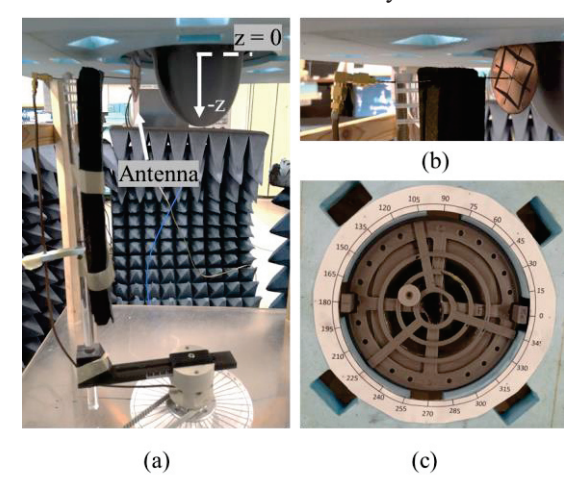


Fig. 1. MW setup: (a) XETS antenna directed to a breast phantom placed in a styrofoam base (b) XETS antenna (c) top view of the breast phantom.

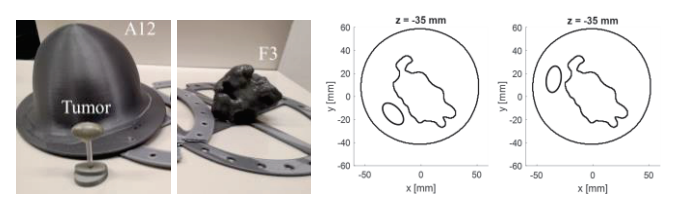


Fig. 2. Breast phantom containers: breast (A12), fibroglandular (F3) and tumor, and two tumor positions: (left) Position 1, (right) Position 2.

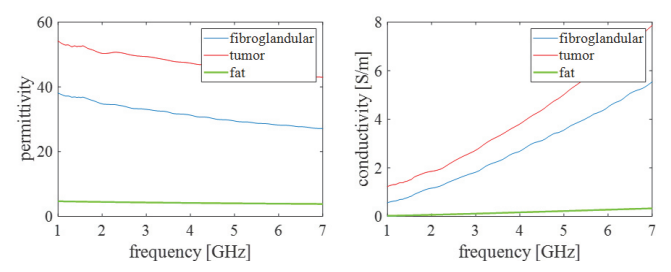


Fig. 3. Permitivitty and conductivity of fat, fibroglandular and tumor.

We measure the input reflection coefficient, $s_{11}(f)$, at every 9°, in a total of 40 observations points over a circumference around the breast. Moreover, during the scan and considering the z-plane of the antenna, the minimum, maximum and average distances between the antenna and the breast were of 20.9 mm, 38.8 mm and 28.5, respectively.

This work was performed using only one breast phantom and a target, which mimics a tumor. The tumor was placed in two different positions inside the breast phantom, one at a time, as depicted in Fig. 1 (c). The position of the tumor and the antenna were kept in the same z-plane, z = -35 mm.

B. Breast and tumor phantoms

For this experimental work, we created a breast phantom, using the MRI-derived breast model repository obtained from the University of Manitoba [6]. We 3D-printed a breast shell (A12), as depicted in Fig. 2, with 1.2 mm wall thickness, using polylactic acid (PLA, $\varepsilon_r = 2.75 - j0.03$ at 4 GHz [7]) on an Ultimaker 3 Extended [8]. This shell represents the skin of the breast. Although the dielectric properties of PLA are different to the ones of skin it enables fast prototyping and testing. Moreover, this approximation does not change the nature of the MW scattered signals, not affecting this study in a critical manner. To represent the fat tissue of the breast, we filled this shell with Triton X-100 (TX-100) which approximates the dielectric properties of fat.

Using the same methodology, as seen in Fig. 2, we also 3D-printed an anthropomorphic shell (F3), from the same repository, that mimics fibroglandular tissue and an ellipsoidal tumor container with a 10 mm larger radius. Both containers were also filled with specific mixtures [9] that represent typical fibroglandular and tumor properties, and then were inserted inside the breast shell (with the fat liquid – TX-100). In Fig. 3, we present the permittivity and conductivity of these mixtures, as well as of the fat liquid, all measured with the open-ended coaxial probe method [10].

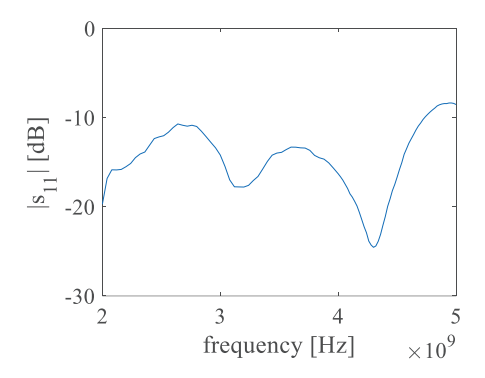


Fig. 4. Input reflection coefficient of antenna in free-space, $s_{11}(f)$.

The tumor was placed in two different positions inside the breast. With Fig. 2, we show the localization of those positions, as well as the shape of the fibroglandular tissue and of the breast in the z-plane being considered. For reference, notice that, in terms of area, the fibroglandular tissue occupies 20.7% of the space inside the breast.

C. Microwave imaging reconstruction algorithm

To remove the response of the antenna XETS from the $s_{11}(f)$ signals, we start by subtracting a measurement of the antenna in free space, depicted in Fig. 4, as explained in [5].

When analyzing the collected $s_{11}(f)$ signals, we notice an intense and first reflection from the skin of the breast. Hence, prior to the imaging of the breast, we apply an adaptive artifact removal algorithm, based on singular value decomposition [4], which uses the signal similarity between consecutive antennas to remove these reflections.

The artifact removal is followed by the image reconstruction algorithm based on wave-migration [4]. This algorithm uses the geometry of the breast to migrate the propagating wave from the antenna to the synthetical focal point in the breast. The contributions from all antenna positions a and frequency points f are summed for each pixel p and organized in a 2D-matrix (image), according to the following expression:

$$I(x,y) = \left| \sum_{a} \sum_{f} s_{11}(f,a) e^{2jk_0(f)(d_b n_b + d_{air})} \right|^2$$
 (1)

where j is the imaginary unit, $k_0(f) = 2\pi f/c$ is the wavenumber in vacuum, d_b is the distance travelled inside the breast, d_{air} is the one travelled in air, n_b is the refractive index of fat and I_p represents the magnitude of the pixel at coordinate (x, y).

To assess the quality of an image, besides visually inspection, we used a quantitative figure of merit.

1) Tumor-to-clutter ratio (TCR): compares the maximum intensity corresponding to the tumor response (T) and the larger unwanted artifact intensity (clutter - C) occuring in the 2D image being considered:

$$TCR [dB] = 10 \log_{10} \left[\frac{\max (T)}{\max (C)} \right]$$
 (2)

III. ANTENNA POSITIONS ASSESSMENT

Considering that in a monostatic system, the antenna is moving around the breast, collecting signals at different angular positions, the more positions we consider, the more time is needed to perform the exam. However, it is possible that after a certain number of positions, the image does not benefit from adding more antenna positions. To assess this trade-off, Fig. 5 shows the imaging results and corresponding TCR for the breast phantom, considering the two tumor positions, and 40, 20 and 10 regularly distributed angular positions. All other parameters were kept constant.

We notice that all imaging results have a lot of artifacts, thus the negative calculated TCR. As proved in a previous work by the authors [11] this is due to the irregular shape and volume of the fibroglandular structure. However, it is noticeable that using 40 angular positions does not improve much the imaging results compared to 20 angular positions, but it would double the time to perform the scan. Moreover, performing only 10 angular positions decreases substantially the image quality. These results are supported by the TCR calculated values. In fact, although we are in a near-field scenario, these results are aligned with the Synthetic Aperture Radar (SAR) azimuth resolution for far-field that states that the maximum resolution is fixed at D/2, where D is the antenna length [12] (5 cm for the case of the XETS).

Another configuration related with the antenna that could be optimized is the distribution of antenna positions around the breast. Usually, researchers use equidistant angular

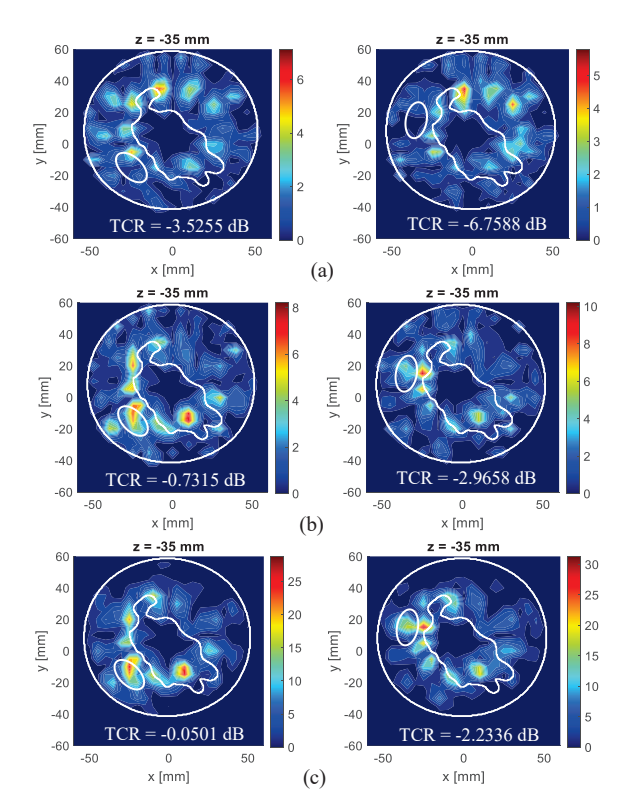


Fig. 5. Two-dimensional images obtained using one anthropomorfic breast phantom with two possible tumor positions. MWI using (a) 10 (b) 20 (c) 40 angular position.

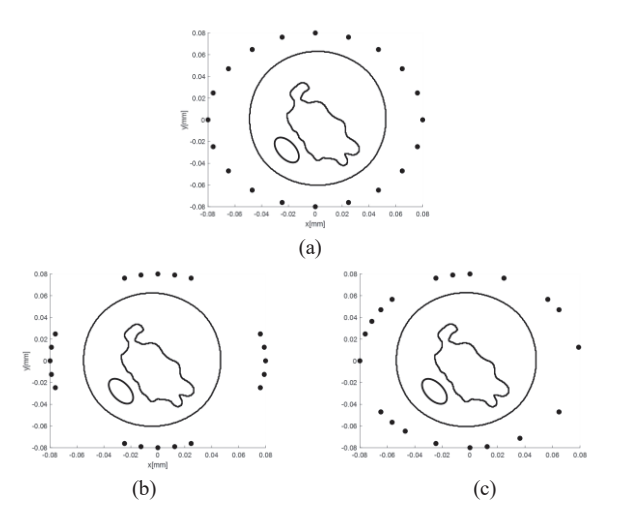


Fig. 6. Different layouts for 20 antennas: (a) Layout 1 (b) Layout 2 (c) Layout 3.

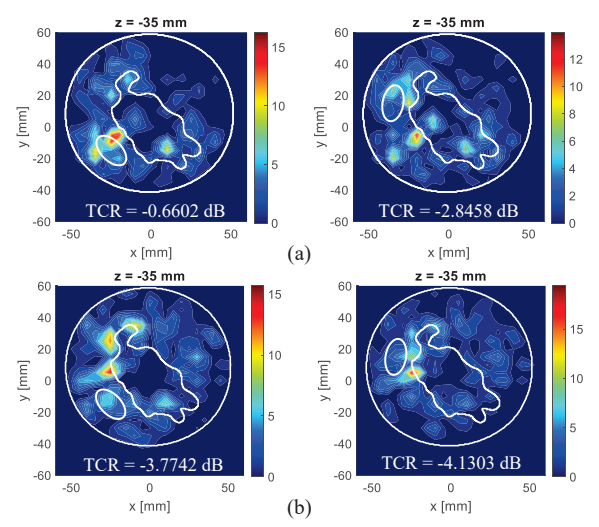


Fig. 7. Two-dimensional images obtained using one anthropomorfic breast phantom with two possible tumor positions, 20 antenna positions. MWI using (a) Layout 2 (b) Layout 3.

positions, i.e., the distance between consecutive antenna positions is always the same, as depicted in Fig. 6 (a) as "Layout 1". However, it is known that for symmetric breasts, this configuration can lead to high intensity values inadvertently. Hence, in this work, we tested other types of layouts, to see if they would improve image quality. These are depicted in Fig. 6 (b) and (c). In the first case, the chosen 20 antenna positions are retrieved from four groups with a lower spacing between then, and in the last case, the 20 antennas positions are randomly chosen from the original 40, originating a random spacing between them.

Fig. 7 show the imaging results and the TCR metric, obtained for these two new layouts. As we can see, the artifacts introduced by the fibroglandular tissue are still visible, although it has reduced compared with Layout 1 (Fig. 5 (b)). Although, Layout 2 performed slightly better tumor detection than Layout 1, Layout 3 did not show any improvement.

IV. FREQUENCY POINTS ASSESSMENT

Similar to what was performed in the last section, in here we study the impact of frequency band on tumor detection. In a primary test, we show in Fig. 8 imaging results using different number of frequency points (51, 76 and 151) for the considered band, [2-5] GHz. As usual, TCR metric results are also displayed.

Using visual inspection and looking at the TCR results, we can state that although the signal acquisition was made with 151 points, we can decrease the number of points while keeping a small variance in the metrics, thus decreasing the examination time.

Researchers on the topic of breast cancer, usually use frequencies between 2 to 7 GHz in their MWI systems [13]. This is because lower frequencies allow for better tissue penetration, while higher frequencies enable better image resolution. Next, we divide our bandwidth in half to check if the lower or higher frequencies alone were benefiting image quality. Hence, Fig. 9 shows the imaging results and corresponding TCR obtained for two new bandwidths [2-3.5] GHz and [3.5-5] GHz.

From the poor imaging results, we can assume that we may need a larger bandwidth. Hence, Fig. 10 (a) e (b) depicts the imaging results obtained when we increase these bandwidths by 0.5 GHz ([2-4] GHz and [3-5] GHz). For consistency, in Fig. 10 (c) we also explore the use of a bandwidth which is the junction between [2-3] GHz and [4-5] GHz.

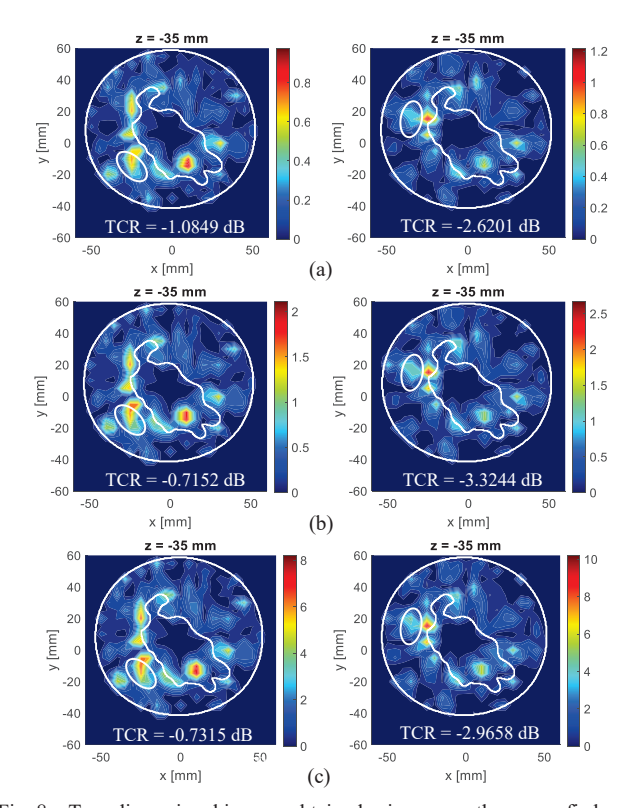


Fig. 8. Two-dimensional images obtained using one anthropomorfic breast phantom with two possible tumor positions. MWI using [2-5] GHz with (a) 51 (b) 76 (c) 151 frequency points.

By looking at the TCR metric, it is noticeable that the optimal frequency for this system is between [2-4] GHz. The information of the tumor seems to be captured in the frequency range [3-4] GHz. However, it looks like it's more useful when combined with lower frequencies than with higher frequencies. This is not only visible with the TCR metric, but also comparing Fig. 10 (a) and (b).

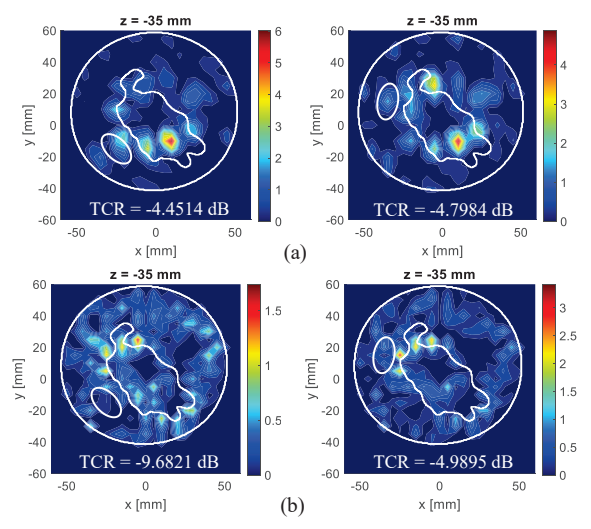


Fig. 9. Two-dimensional images obtained using one anthropomorfic breast phantom with two possible tumor positions. MWI using 76 frequency points (a) [2-3.5] GHz (b) [3.5-5] GHz.

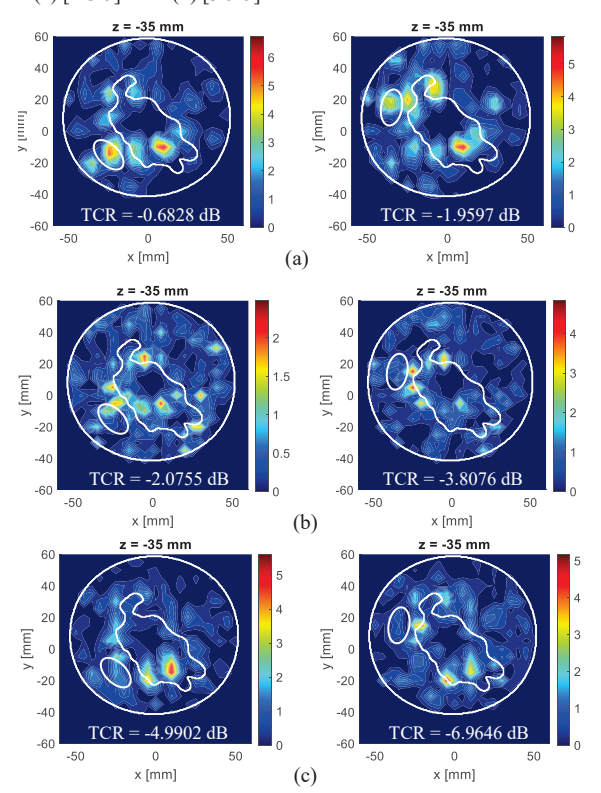


Fig. 10. Two-dimensional images obtained using one anthropomorfic breast phantom with two possible tumor positions. MWI using 101 frequency points (a) [2-4] GHz (b) [3-5] GHz (c) [2-3] GHz + [4-5] GHz.

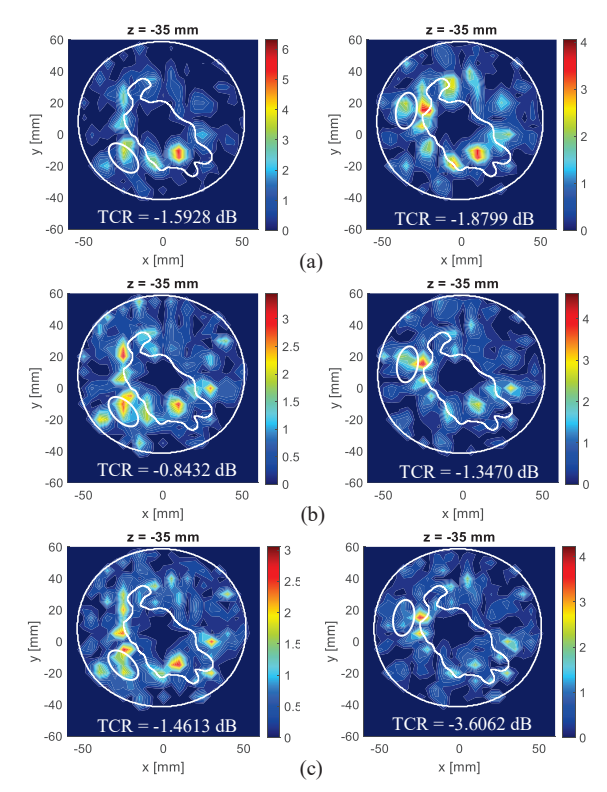


Fig. 11. Two-dimensional images obtained using one anthropomorfic breast phantom with two possible tumor positions. MWI using [2-5] GHz with different concentration of points for each individual Ghz (a) ½-¼-¼ (b) ¼-½-¼ (c) ¼-¼-½-½.

Next, we analyze what happens when we give more importance to some bandwidths than others, instead of not considering them at all. In the last tests, each individual GHz had the same number of points. Now, we study the idea of having different concentration of points throughout the whole bandwidth. Fig. 11 depicts the imaging results and TCR. As an example, consider the ½-¼-¼ configuration, this means that there will be 51 points in the [2-3] GHz band, 25 in the [3-4] GHz band and 25 in the [4-5] GHz band, in a total of 101 points. As before, a higher concentration of points in the middle GHz band showed better TCR results while higher concentration of points in the high frequency band did not show much improvement.

V. CONCLUSIONS AND FUTURE WORK

This paper presented a systematic study to understand if optimizing certain configurations related with the antenna and frequency band of a MWI system can have an impact on tumor detection, while also improving acquisition time.

To this end, we performed measurements in a dry MW experimental setup, using a XETS antenna working in a monostatic configuration, in the frequency range of 2-5 GHz, moving around an anthropomorphic breast phantom, with two possible tumor positions. With the collected signals we built images using a wave-migration algorithm and with visual assessment and a quantity metric, we interpreted the results.

With this work, we understood that there is a specific number of angular positions and frequency points from which the quality of imaging results does not increase substantially. Meaning that, if we optimize these parameters in advance, a crucial amount of acquisition time can be recovered. We also found the optimal frequency band and showed that higher frequencies may not be very useful. This should be further explored with different anthropomorphic breasts. Moreover, a layout of antenna positions different from the usual circular equidistant one, could potentially improve tumor detection. So, different layouts should be investigated in the future.

ACKNOWLEDGMENT

This work was funded by Fundação para a Ciência e Tecnologia (FCT/MCTES) through national funds under scholarship SFRH/BD/144961/2019, and in part by FEDER under projects UIDB/50008/2020 and 2022.04764.PTDC (IRMIS).

REFERENCES

- [1] N. K. Nikolova, "Microwave Imaging for Breast Cancer," *IEEE Microwave Magazine*, vol. 12, no. 7, pp. 78-94, Dec. 2011.
- [2] E. C. Fear, et al., "Microwave Breast Imaging With a Monostatic Radar-Based System: A Study of Application to Patients," *IEEE Transactions on Microwave Theory and Techniques*, vol. 61, no. 5, pp. 2119-2128, May 2013.
- [3] S. Kwon, and S. Lee," Recent Advances in Microwave Imaging for Breast Cancer Detection," *Int. J. Biomed. Imaging*, ID 5054912 pp. 1-26, 2016.
- [4] J. M. Felício, et al., "Microwave Breast Imaging using a Dry Setup," IEEE Trans. Comput. Imaging, vol. 6, no. 1, pp. 167-180, Jan., 2020.
- [5] J. M. Felício, et al., "Antenna Design and Near-field Characterization for Medical Microwave Imaging Applications," *IEEE Trans. Antennas Propag.*, vol. 67, no. 7, pp. 4811 - 4824, July, 2019.
- [6] T. Reimer, et al., "An Open-Access Experimental Dataset for Breast Microwave Imaging," 2020 14th European Conference on Antennas and Propagation (EuCAP), 2020, pp. 1-5.
- [7] J. M. Felício, et al., "Complex permittivity and anisotropy measurement of 3D-printed PLA at microwaves and millimeter-waves," *Proc. 22nd Int. Conf. Appl. Electromagn. Commun. (ICECOM)*, Dubrovnik, Croatia, Sep. 2016, pp. 1–6.
- [8] Ultimaker, "Professional 3D printing made accessible-Ultimaker," 2022. [Online]. Available: https://ultimaker.com/.
- [9] N. Joachimowicz, et al., "Breast Phantoms for Microwave Imaging," *IEEE Antennas and Wireless Propagation Letters*, vol. 13, pp. 1333– 1336, 2014.
- [10] J. S. Bobowski and T. Johnson, "Permittivity measurements of biological samples by an open-ended coaxial line," *Prog. Electromagn. Res. B*, vol. 40, pp. 159–183, 2012.
- [11] R. A. Martins, et al., "Study of the Effect of Fibroglandular Tissue in Tumor Detection Using Microwave Breast Imaging," 2023 17th European Conference on Antennas and Propagation (EuCAP), Florence, Italy, 2023, pp. 1-4.
- [12] M. T. Crockett and D. Long. "An Introduction to Synthetic Aperture Radar: a High-Resolution Alternative to Optical Imaging." (2013).
- [13] J. M. Felício, R. A. Martins, J. R. Costa, Overview of Microwave Breast Imaging for Cancer Screening, *IEEE Antennas and Propagation Magazine* (submitted and acepted).